

# Growth kinetics in position-controlled and catalyst-free InAs nanowire arrays on Si(111) grown by selective area molecular beam epitaxy

S. Hertenberger, D. Rudolph, M. Bichler, J. J. Finley, G. Abstreiter, and G. Koblmüller<sup>a)</sup>  
*Walter Schottky Institut and Physik Department, Technische Universität München, Garching,  
 85748, Germany*

(Received 5 August 2010; accepted 9 November 2010; published online 14 December 2010)

We investigated the interwire distance dependence on the growth kinetics of vertical, high-yield InAs nanowire arrays on Si(111) grown by catalyst-free selective area molecular beam epitaxy (MBE). Utilizing lithographically defined SiO<sub>2</sub> nanomasks on Si(111) with regular hole patterns, catalyst-free and site-selective growth of vertically (111)-oriented InAs nanowires was achieved with very high yields of  $\sim 90$  percent. Interestingly, the yield of vertically ordered nanowires was independent of the interwire distance and the initial growth stages. Significant size variation in the nanowires was found to depend critically on the interwire distance and growth time. Two growth regimes were identified—(i) a competitive growth regime with shorter and thinner nanowires for narrow interwire distances and (ii) a diffusion-limited growth regime for wider distances, providing good estimates for the surface diffusion lengths. Surprisingly, despite these size-dependent effects the nanowire geometries remained unaltered with uniform, almost nontapered morphologies even over large variation in nanowire density ( $\sim \text{mid}-10^6\text{--}10^9 \text{ cm}^{-2}$  range). X-ray diffraction further confirmed the vertical (111) directionality with low crystal tilt by rocking curve widths ( $\omega$  scans) as low as  $\sim 0.6^\circ$ . These findings demonstrate the capability to precisely tailor the position and size of well-oriented III-V semiconductor nanowires through noncatalytic MBE selective area growth and provide an important step toward fully integrated, uniform vertical III-V nanowire array-on-Si devices. © 2010 American Institute of Physics. [doi:10.1063/1.3525610]

## I. INTRODUCTION

Semiconductor nanowires currently attract much attention due to their unique geometries and functional properties with heterostructures,<sup>1,2</sup> that provide rich prospects for novel electronic and optoelectronic devices,<sup>3,4</sup> solar cells,<sup>5,6</sup> thermoelectric devices,<sup>7,8</sup> and biosensors.<sup>9</sup> In particular, InAs nanowires are of great interest due to their low band gap energy ( $E_g \sim 0.36 \text{ eV}$ ), small electron effective mass, and high electron mobility ( $\mu \sim 33\,000 \text{ cm}^2/\text{V s}$  at 300 K). These properties make them predestined for future high-speed electronic and near-infrared photonic devices.<sup>10-12</sup> In addition, high-performance cost-effective III-V nanowires on a silicon (Si) platform are long-sought after, since they directly address the vision of monolithic integration in semiconductor technology and may circumvent the problems associated with the large lattice mismatch ( $\sim 11.6\%$  for InAs on Si) during III-V heteroepitaxy on Si.<sup>13</sup>

For functional nanowire devices it is essential to have control over position, size, directionality, and microstructure of the nanowires in order to allow their implementation into large-scale homogeneous arrays with predictive performance. Simultaneously, the growth of device-quality nanowires with high purity should further abstain from common nucleation schemes that employ foreign catalysts such as gold. Gold is well known to introduce deep level traps in the semiconductor band gap, limiting the performance of functional III-V-on-Si devices.<sup>14,15</sup> To meet all these demands, there has been only a limited amount of success for III-As-

based nanowires on Si, mainly via selective area epitaxy (SAE) using methods such as pulsed laser deposition, chemical beam epitaxy, and metal organic chemical vapor deposition (MOCVD).<sup>16-18</sup> While these reports demonstrated good control of nanowire position, directionality, and size, they relied on predefined gold-droplet nucleation sites and the growth kinetics were restricted to the vapor-liquid-solid growth mechanism.

In contrast, during noncatalytic growth methods control of preferential growth directionality was difficult to achieve due to the crucial polar/nonpolar nature of the group-III-As/Si(111) heterointerface.<sup>19</sup> However, Tomioka *et al.*<sup>20</sup> highlighted much improved vertical directionality of position-controlled InAs nanowires on template-masked Si(111) substrates via manipulation of the initial growth stages during MOCVD growth processes. The same group has also demonstrated size-control of SAE grown InAs nanowires by variation in growth parameters (temperature) on various substrates, such as partially masked InAs (111)B, InP, and GaAs (111)B.<sup>19,21,22</sup>

Despite these advances, no investigations have yet been performed that directly address the crucial interplay between nanowire position (i.e., interwire distance), growth kinetics, and related size effects in III-As-based nanowires on Si during noncatalytic growth processes. These critical parameters should deliver key knowledge to catalyst-free SAE induced nanowire growth in general.

Moreover, little attention has been paid to SAE growth of group-III-As based nanowires by growth techniques other than those mentioned above. This is due to the general ad-

<sup>a)</sup>Electronic mail: gregor.koblmueeller@wsi.tum.de.

vantage of chemical vapor phase (CVD) techniques, where the selectivity is mainly governed by the much lower gas phase reactivity and higher desorption on masked dielectric layers as compared to the semiconductor surface. For techniques that use elemental (atomic) sources, such as solid-source molecular beam epitaxy (MBE), growth selectivity is typically more restricted since group-III atoms do not desorb readily once they are adsorbed. This makes it more difficult to perform SAE growth at low temperatures as compared to (MO)-CVD methods, limiting selective area MBE growth to conditions only where sufficient surface diffusivity can be achieved. In addition, MOCVD and related gas phase techniques typically offer higher surface diffusion, faster growth rates and higher throughput. However, solid-source MBE is expected to exploit several advantages such as low impurity incorporation from the ultrahigh vacuum environment and highly pure elemental growth species, very accurate composition and doping control and the ability to grow advanced core-shell heterostructures via sophisticated *in situ* growth monitoring methods.<sup>23–26</sup> Recently, solid-source MBE growth of self-assembled free-standing InAs nanowires on Si has been demonstrated<sup>27,28</sup> but no investigations of SAE growth of free-standing group-III-As nanowires on Si by MBE have been reported so far.

In this study, we investigated various growth kinetics effects during catalyst-free, selective area growth of vertical InAs nanowire arrays by solid-source MBE on lithographically defined Si(111) substrates. Based on differences in the size scaling behavior, we demonstrated the existence of two growth regimes as a function of interwire distance (latter also referred to as pitch), i.e., a competitive growth regime for small distances and a diffusion-limited growth regime for large distances. Interestingly, as opposed to catalytically grown nanowires, we found also significant nonlinearity in the growth rate over growth time with non-negligible radial growth rates that depended on the interwire distance. Overall, we demonstrated that in the MBE-grown InAs nanowires excellent growth selectivity with very high yields of  $\sim 90$  percent (i.e., ratio of vertically aligned InAs nanowires per predefined nucleation site) was possible—which was independent of prewetting, initial growth stages, and the selected interwire distance. For consistency with our growth kinetics studies describing the growth of vertically well aligned InAs nanowire arrays, we confirmed their near-perfect alignment by a very low crystal tilt as measured by x-ray diffraction (XRD).

## II. EXPERIMENTAL DETAILS

All growth was performed in a Gen-II MBE system equipped with several cryopumps to guarantee high purity growth conditions, standard effusion cells for group-III elements (Al, Ga, and In) and a Veeco valve cracker cell supplying arsenic ( $\text{As}_4$ ). A pyrometer was used to measure the substrate temperature *in situ* during growth. The supplied In fluxes are expressed in equivalent (111) InAs thin film growth rate units ( $\text{\AA}/\text{s}$ ), calibrated by reflection-high energy electron diffraction. Further details on the growth and flux calibration are reported elsewhere.<sup>28</sup>

The InAs nanowires were grown on commercially available p-doped Si(111) wafers. SAE was realized via a thin nanomask consisting of 20 nm thermal  $\text{SiO}_2$ , where hole structures with opening diameters (40–100 nm) and pitches (250–5000 nm) were predefined in a 100 nm thick photo resist using a Raith “e-line” electron-beam lithography system. Sample processing optimization required a quick  $\text{O}_2$ -plasma-etching step after development to obtain accurate cylindrical holes. Subsequent reactive ion etching (RIE) transferred the pattern into the  $\text{SiO}_2$  mask and made the wafers ready for liftoff and a second  $\text{O}_2$ -plasma-etching cycle to remove remaining resist. To get rid of all kinds of contaminants and to provide a clean oxide-free Si surface within the holes, the entire wafers were etched in an aqueous hydrofluoric (HF) solution reducing the  $\text{SiO}_2$  to a final thickness of  $\sim 18$  nm prior to nanowire growth. Immediately afterwards the wafers were loaded to the MBE and annealed at 770 °C for 15 min.

Growth was then performed after subsequent cool-down to substrate pyrometer temperatures of 460–520 °C, employing an In-flux rate of 0.24  $\text{\AA}/\text{s}$  and  $\text{As}_4$  beam equivalent pressure (BEP) of  $2.6 \times 10^{-6}$  mbar ( $=1.5 \text{\AA}/\text{s}$ ) unless otherwise noted. Three distinct nanowire growth studies were performed: (i) under variable growth temperature to identify the growth selectivity, (ii) by variation of hole diameter and pitch of the prepatterned  $\text{SiO}_2/\text{Si}(111)$ , and (iii) by variation in growth time at fixed hole diameter of 80 nm. The as-grown nanowire samples were then investigated by scanning electron microscopy (SEM) for growth selectivity, nanowire morphology, their diameters and lengths. All SEM images shown in this study were recorded at a tilt angle of 54°. Double-crystal high-resolution x-ray diffraction (HRXRD) in a Philips X’Pert Pro MRD diffractometer was further employed to determine the crystalline quality and vertical (111) directionality, i.e., crystal tilt, from rocking curve peakwidths ( $\omega$  scans).

## III. RESULTS AND DISCUSSION

### A. Growth selectivity and vertical nanowire growth yield

The InAs growth selectivity depended critically on the growth temperature. This was characterized by the morphological properties in the vicinity of a single prepatterned hole (diameter of 80 nm, pitch 5  $\mu\text{m}$ ) after growths were performed in the temperature range of 460–520 °C (Fig. 1). For the given As-flux (i.e., 1.5  $\text{\AA}/\text{s}$ ), growth at a temperature of 460 °C resulted in nanowire formation at the predefined hole but also in large InAs cluster coverage on the  $\text{SiO}_2$  surface due to reduced surface diffusion at this temperature [Fig. 1(a)]. In contrast, at 480 °C surface diffusion on  $\text{SiO}_2$  was significantly increased, yielding much lower sticking probability of In on  $\text{SiO}_2$  and hence InAs nanowires nucleated only at the predefined holes [see Fig. 1(b)]. Note, that the length of the nanowires was reduced from  $\sim 1.0 \mu\text{m}$  (460 °C) to  $\sim 0.85 \mu\text{m}$  (480 °C). For growth temperatures higher than 480 °C, the selectivity was still perfectly realized but the nanowire lengths were reduced much more significantly ( $\sim 0.52 \mu\text{m}$ ) for 505 °C [Fig. 1(c)] and merely

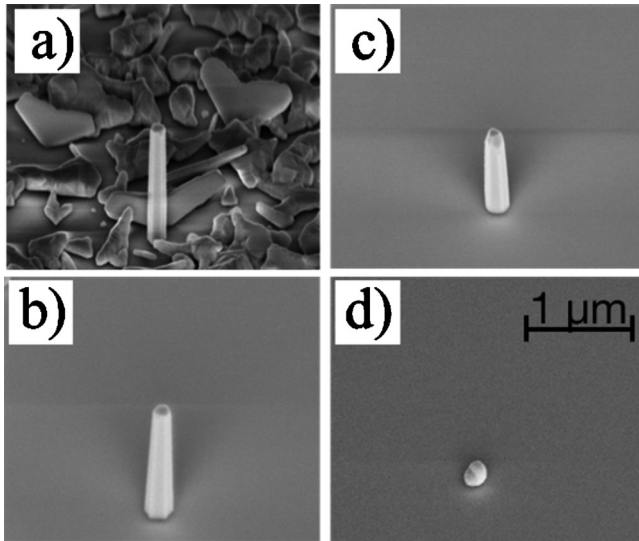


FIG. 1. SEM micrographs showing the area around a predefined hole (lithographically patterned with diameter of 80 nm and pitch of 5  $\mu\text{m}$ ) after growths performed at different substrate temperatures ranging from (a) 460  $^{\circ}\text{C}$  to (b) 480  $^{\circ}\text{C}$ , (c) 505  $^{\circ}\text{C}$ , and (d) 520  $^{\circ}\text{C}$ . The growth conditions were otherwise constant with  $\text{In}=0.24$   $\text{\AA}/\text{s}$  and  $\text{As}=1.5$   $\text{\AA}/\text{s}$  (BEP of  $2.6 \times 10^{-6}$  mbar). Note the trade-off between selectivity and nanowire length as a function of temperature.

InAs droplets for 520  $^{\circ}\text{C}$  [Fig. 1(d)]. This characteristic length dependence on substrate temperature was previously observed and associated with enhanced thermal dissociation rates at higher temperatures.<sup>28</sup> We conclude that nanowire growth with good selectivity takes place in a small temperature window between  $\sim 480$ – $510$   $^{\circ}\text{C}$ . These observations mimic previous studies utilizing selective growth effects on  $\text{SiO}_2$  masked substrates.<sup>19,29–33</sup>

Based on the trade-off between selectivity and nanowire length, we have selected an optimum substrate temperature of 480  $^{\circ}\text{C}$  for all consecutive growth experiments. Figure 2

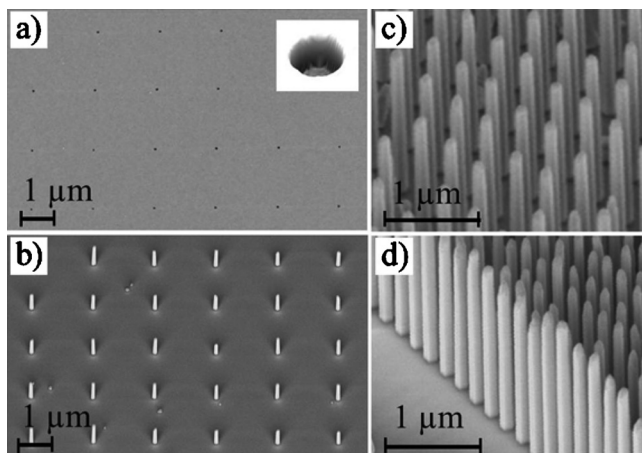


FIG. 2. (a) AFM image of a prepatterned  $\text{SiO}_2/\text{Si}(111)$  substrate. The holes were 18 nm deep, had a diameter of 80 nm and a distance (pitch) of 2  $\mu\text{m}$  between each other. The magnified area (inset) shows a 3D AFM image of a single hole. (b) Tilted SEM image of 45 min MBE grown InAs nanowires on a  $\text{SiO}_2/\text{Si}(111)$  substrate as prepared in (a) at As-BEP of  $2.6 \times 10^{-6}$  mbar. (c, d) SEM images of InAs nanowires grown for 90 min with a higher As-BEP of  $5.2 \times 10^{-6}$  mbar and a pitch of 500 nm (c) and 250 nm (d), respectively. The SEM micrograph shows the edge of the patterned field and demonstrates the excellent selectivity.

illustrates that this temperature provided excellent selectivity and vertical growth yield for a range of pitches and In/As-flux ratios. More in detail, Fig. 2(a) shows an atomic force microscope (AFM) image of a representative patterned  $\text{SiO}_2/\text{Si}(111)$  wafer with 80 nm wide openings (holes) and a pitch of 2  $\mu\text{m}$ . The holes were processed as described in the previous section and had a depth of 18 nm. The magnified image (inset) illustrates a three-dimensional (3D) AFM image of a single hole, further demonstrating its cylindrical geometry. The SEM image shown in Fig. 2(b) evidences that all InAs nanowires nucleated at the predefined nanomask pattern (i.e., pitch of 2  $\mu\text{m}$ ) when grown under identical As-flux conditions as before (1.5  $\text{\AA}/\text{s}$ ). The nanowires had average diameters of 233 nm ( $\pm 8$  nm) and lengths of 1  $\mu\text{m}$  ( $\pm 57$  nm). Furthermore, all nanowires exhibited hexagon-shaped cross-section with surrounding  $\{110\}$  side facets, similar to recent observations for nonselectively grown InAs nanowires.<sup>28</sup> Figures 2(c) and 2(d) show electron micrographs of InAs nanowires grown for 90 min with a higher As-flux (i.e., 3  $\text{\AA}/\text{s}$ , BEP of  $5.2 \times 10^{-6}$  mbar) at two different pitches—i.e., 500 nm pitch [Fig. 2(c)] and 250 nm pitch [Fig. 2(d)]. Figure 2(d) was recorded at the edge of the patterned field and shows the intersection between unpatterned and patterned  $\text{SiO}_2$  underlining further the very good growth selectivity. These growths resulted in nanowires with identical average diameters of 131 nm and lengths of 1.71  $\mu\text{m}$ , which is an increase in aspect ratio (length/diameter) by a factor of two compared to nanowires grown at the low As-flux conditions with comparable pitch. This indicates that the vertical nanowire growth rate scales linearly with the supplied  $\text{As}_4$  flux, similar to recent observations for MBE-grown GaAs nanowires.<sup>34</sup>

The vertical nanowire yield of the growths presented in Fig. 2 averaged over  $\sim 300$  holes was 90 percent. The crucial finding to obtain nanowire arrays with such high yield depended on accurate pattern processing, including precise etching of the holes, but much less on nucleation conditions. Different attempts were carried out to vary nucleation conditions based on the relative time period between  $\text{As}_4$  and Indium supply (i.e.,  $t_{\text{As}} - t_{\text{In}}$ ). In detail, we selected a time variation in  $\text{As}_4$  supply ranging from 30 min before opening to 20 s after opening of the In shutter. This can be referred to as  $\text{As}_4$  preannealing ( $t_{\text{As}} - t_{\text{In}} < 30$  min), simultaneous In/ $\text{As}_4$  supply ( $t_{\text{As}} - t_{\text{In}} = 0$ ), and In prewetting ( $t_{\text{In}} - t_{\text{As}} < 20$  s). The time period for the In prewetting experiment correlates to an equivalent In coverage of less than  $\sim 3$  MLs.  $\text{As}_4$  preannealing was also carried out at different substrate temperatures ranging from 350–480  $^{\circ}\text{C}$ .

For all these different prewetting conditions, we observed no effect on the ratio of vertically aligned InAs nanowires. This indicates larger independence of the vertical growth yield to the prewetting conditions and the polar/nonpolar nature of the InAs/Si(111) heterointerface as previously identified in Ref. 20. In this report, which was based on noncatalytically grown InAs nanowires by MOCVD, a significant ratio of nanowires grew along three equivalent inclined (111)B-orientations [i.e., tilted by 19.6 $^{\circ}$  to the Si(111) surface]—a common observation in III-V nanowires on Si.<sup>13,17,35</sup> Via refined modulated  $\text{AsH}_3/\text{H}_2$  prewetting con-

ditions at low temperature very high vertical nanowire growth yield could be achieved.<sup>20</sup> The difference with the current work may be related to the different surface chemistries in MBE and MOCVD processes, i.e., hydrogen and carbon containing precursors in MOCVD versus atomic III elements and molecular  $\text{As}_4$  in MBE processes. Molecular  $\text{As}_4$  is known to readily desorb at temperatures above  $\sim 250^\circ\text{C}$  in UHV environment,<sup>36</sup> therefore, the time period of  $\text{As}_4$  supply relative to In shuttering should have no influence on the surface kinetic properties during nanowire nucleation in MBE. Furthermore, comparison among different patterned fields with different pitches (such as in Fig. 2) resulted in consistently identical growth yields. This further implies significant independence of the growth yield from the interwire distance and corresponding surface diffusion kinetics.

On the other hand, we stress the importance of optimized pattern processing. In fact, we observed a threefold increase in vertical nanowire growth yield from initially  $\sim 30\%$  to finally  $\sim 90\%$  by careful etching of the predefined holes. RIE etching with depths exceeding those of the  $\text{SiO}_2/\text{Si}(111)$  interface (i.e., etching into the Si substrate) resulted in poor vertical nanowire growth yields as compared to accurate etching very close to the interface. In addition, remaining  $\text{SiO}_2$  within the predefined holes led to poor selectivity and very limited nanowire growth.

## B. Vertical directionality and crystal tilt

To evaluate the epitaxial relationship and the large-scale, homogeneous directionality for the vertically aligned InAs nanowires with respect to the Si(111) substrate, we performed HRXRD measurements on selected samples. In Fig. 3(a) a representative HRXRD  $2\theta-\omega$  scan is shown for the sample from Fig. 2(b), demonstrating that no other reflections than those associated with the c-InAs (111) (i.e.,  $25.3^\circ$ ) and the Si(111) orientations (i.e.,  $28.4^\circ$ ) were observed. This indicates the direct epitaxial relationship between the InAs nanowires and the Si substrate, i.e.,  $\text{InAs}[111]\parallel\text{Si}[111]$ . Also, similar to previous investigations<sup>27,28</sup> the predominant reflection at  $2\theta=25.3^\circ$  was associated with zincblende crystal structure, while no peaks were observed at the dominant wurtzite reflections typically occurring at  $2\theta=24^\circ$  (100),  $25.4^\circ$  (002), and  $27.2^\circ$  (101).<sup>28</sup> However, we do not rule out the existence of low volume wurtzite phase or twin defects, considering the resolution limits of HRXRD measurements ( $\sim 10$  arcsec) and the overall low signal peak from low-density nanowire samples.

More importantly, we measured the rocking curve peak width of the InAs (111) reflection ( $\omega$  scans) with open detector and determined a full width at half maximum (FWHM) of  $0.62^\circ$  [Fig. 3(b)]. This was compared with the rocking curve peak width of InAs (111) nanowires grown by standard nonselective (i.e., self-assembled) technique on sputter-deposited  $\text{SiO}_x/\text{Si}(111)$ ,<sup>28</sup> which yielded a FWHM of  $1.24^\circ$ . Although the value measured for the nonselective technique is generally a good indication for well-oriented vertical nanowire arrays with low-crystal tilt, the lower FWHM (factor of 2) for the site-selective grown nanowire arrays proves even more effective suppression of crystal tilt. The low

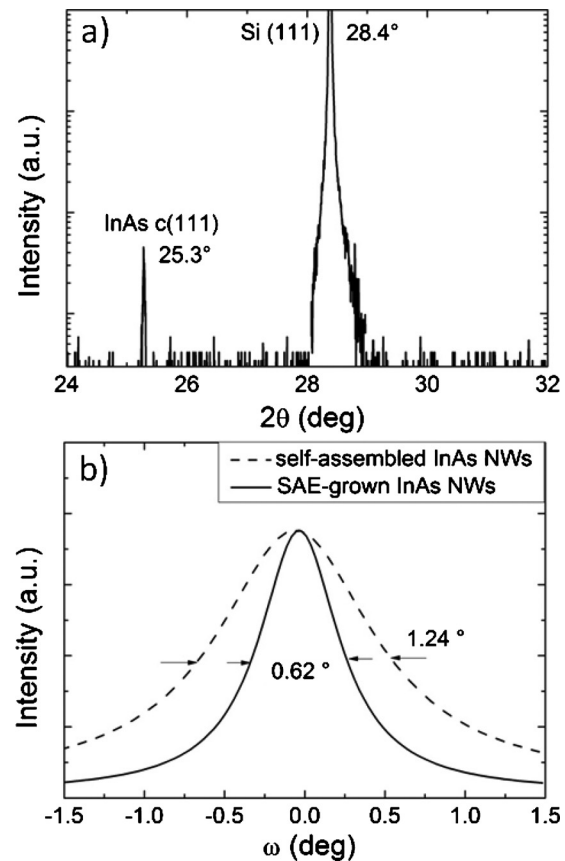


FIG. 3. (a) Double-crystal HRXRD  $2\theta-\omega$  scan of InAs nanowire array from Fig. 1(b) illustrating two peaks associated with c-(111) InAs ( $25.3^\circ$ ) and (111) Si substrate ( $28.4^\circ$ ). (b) Normalized and fitted rocking curves ( $\omega$  scans) of InAs (111) reflection (open detector) for the same site-selectively grown nanowire array in comparison with self-assembled, spatially random nanowire arrays on sputter-deposited  $\text{SiO}_x/\text{Si}(111)$  substrate (Ref. 28).

FWHM value is further in good agreement with the state-of-the-art for the currently best aligned semiconductor nanowire arrays.<sup>37,38</sup> Guaranteeing very low crystal tilt in the vertically well-oriented InAs nanowire arrays was essential for an unobscured analysis of the following growth kinetics effects.

## C. Pitch and growth time dependent nanowire size

In the following, the morphologies and size variation in InAs nanowires grown at standard As-BEP of  $2.6 \times 10^{-6}$  mbar ( $1.5 \text{ \AA/s}$ ) are investigated in more detail with respect to growth time and interwire (pitch) dependence. In Fig. 4, SEM images of positioned free-standing InAs nanowires are shown for different growth times of 10 min (a), 90 min [(b) and (d)], and 360 min (c) at different pitches of 500 nm [(a)–(c)] and  $2 \mu\text{m}$  (d). These different pitches correspond to nanowire densities ranging from  $4 \times 10^8 \text{ cm}^{-2}$  to  $2.5 \times 10^7 \text{ cm}^{-2}$ . We note that we also modified the hole diameters in the range 40–100 nm but found the effect on nanowire diameter to be insignificant. For instance, for a  $1 \mu\text{m}$  wide pitch only a slight increase in nanowire diameter from 133 to 143 nm was observed with increasing hole diameters in the range given above (not shown). The yield for this sample series presented in Fig. 4 was further found independent of growth time and pitch, as discussed earlier.

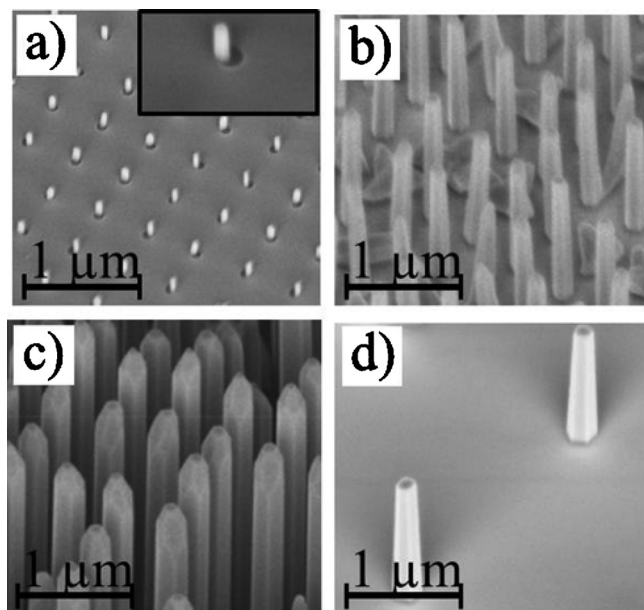


FIG. 4. SEM images of positioned vertically grown InAs nanowires on prepatterned Si(111) with an As-BEP of  $2.6 \times 10^{-6}$  mbar and different growth times of (a) 10 min, (b) 90 min, and (c) 360 min for a constant pitch of 500 nm. Furthermore, InAs nanowires grown for 90 min with a  $2 \mu\text{m}$  pitch are presented in (d). The inset in (a) shows a close-up view of one hole where a small nanowire nucleated at the edge of the hole.

Figure 4(a) provides further insight into the nanowire nucleation characteristics. As growth proceeded only for 10 min, the nanowires resulted in short lengths of 120 nm and diameters of 55 nm. The nanowires are obviously smaller than the holes and the inset shows that they nucleated preferentially at the edge of each hole. This step-edge nucleation behavior is typical for preferential growth of site-selective nanostructures.<sup>39</sup> For longer growth times, the nanowires became longer and thicker and exhibited more whiskerlike geometries, without deteriorating either the underlying hexagonal geometry nor altering the uniformity in diameter and morphology over the entire nanowire lengths [Fig. 4(c)].

To obtain further insight into the different growth kinetics effects, the size scaling behavior of the nanowires with growth time and as a function of pitch is shown in Fig. 5. We found that the lengths of the nanowires scale linearly with time for the larger pitches, while for the smallest pitches, especially the 250 nm wide pitch, the lengths decreased gradually for increased growth time [Fig. 5(a)]. More specifically, for growth times of 10–90 min the length of the nanowires is nearly independent of pitch, whereas for growth times of 180 min and beyond we obtained significantly shorter nanowires for the smallest pitch, indicating a nonlinear evolution of the growth rate as further shown below. Extrapolating the initial time evolution of the nanowire lengths to zero growth time suggests also that the nucleation time before nanowire growth was negligible. Along with the absence of metallic In droplets at the nanowire apex (see all previous SEM images), this gives further evidence for the present noncatalytic nanowire growth mechanism.

The size scaling effects were even more pronounced for the nanowire diameters [Fig. 5(b)], where we observed a nearly linear increase in diameter versus growth time for

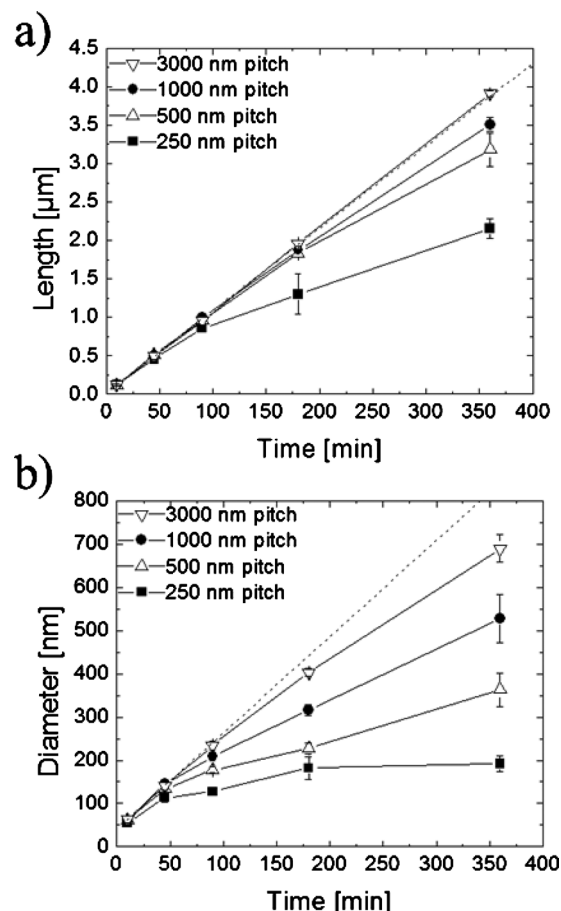


FIG. 5. Nanowire length (a) and diameter (b) as a function of growth time for pitches ranging from 250 nm to  $3 \mu\text{m}$ . Errorbars were determined from averaging 20–30 nanowires per specific sample. The dotted line is a guide to the eye and represents linear growth deduced from extrapolating datapoints for 10 min, 45 min, and 90 min growths.

larger pitches ( $>1 \mu\text{m}$ ). The observation of increasing diameter with growth time is contrasting the typically negligible radial growth of catalytically grown nanowires, where growth is mainly restricted to adatom incorporation via the metallic droplet at the apex of the nanowire.<sup>40</sup> For smaller pitches, however, the increase in diameter was only linear at the beginning of the growth, but saturated quickly after a certain time. For example, at 250 nm pitch the diameter saturated at  $\sim 190$  nm after 180 min and remained constant up to the longest analyzed growth time of 360 min. Although this diameter is very close to the interwire distance (pitch of 250 nm), the nanowires were still free-standing and entirely uncoalesced. Note that the diameters given here were determined by taking the average values at the top and bottom of each nanowire. This approach provided direct information on nanowire tapering [tapering =  $100 \times (\text{top-diameter} - \text{bottom-diameter}) / \text{length}$ ]. The tapering factor as derived from all datapoints presented in Fig. 5 showed no clear dependence with regard to pitch and growth time and was insignificant with 2%–4% on average (max  $< 7\%$ ).

To understand these rate-limiting effects further, we analyzed the axial and radial growth rates as a function of pitch and growth time more closely. The evolution of the growth rates over time, as illustrated in Fig. 6 for a wider range of

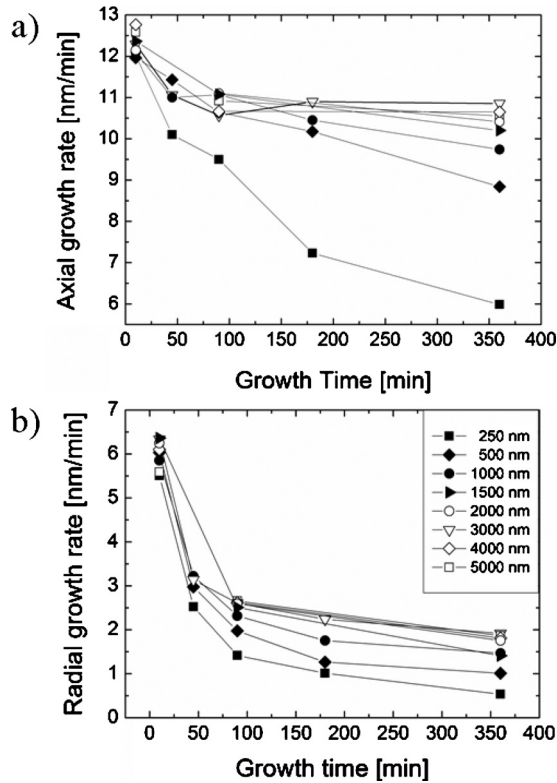


FIG. 6. Time evolution of the (a) axial and (b) radial nanowire growth rates as derived from Fig. 5, indicating the initially higher growth rates during early nucleation and transition to steady-state growth. A clear pitch dependence was observed, shown by decreased growth rates for small pitches ranging from 250–1500 nm (closed symbols) and constant, nearly identical growth rates from larger pitches >1500 nm (open symbols).

itches, shows clearly that nanowire growth was initiated at higher growth rates before reaching steady-state growth. Higher initial growth rates have been observed also for InAs nanowires grown by other methods<sup>18,40</sup> and were associated with the different surface diffusion kinetics on the substrate and nanowire sidewalls. In particular, when the nanowire length ( $L$ ) was shorter than the In adatom diffusion length along the nanowire sidewalls ( $\lambda_{NW}$ ), then the capture area of impinging In adatoms on the nanowire sidewalls increases continuously with time, leading to fast superlinear growth. However, for longer growth times where  $L > \lambda_{NW}$ , the capture area for In adatoms becomes rather constant leading to steady-state growth rates.<sup>18</sup> In addition, we suggest that the initial superlinear growth rate may also stem from the underlying 3D island nucleation characteristics which often show typical power-law growth behavior.<sup>41,42</sup> Nevertheless, upon transition to steady-state growth, the rates depended significantly on the pitch—i.e., the steady-state growth rates were completely identical for pitches above  $\sim 2 \mu\text{m}$  (with constant axial and radial rates of  $\sim 11 \text{ nm/min}$  and  $\sim 2 \text{ nm/min}$ , respectively), while they were less and decreased gradually for lower pitches.

This interesting pitch dependence is a clear evidence of two particular growth regimes defined by the complex interplay between diffusion lengths of In adatoms on  $\text{SiO}_2$  ( $\lambda_{\text{SiO}_2}$ ) and the adatom capture area with respect to selected pitch. Apparently, if the mean diffusion length  $\lambda_{\text{SiO}_2}$  is on the order of or larger than half of the pitch, neighboring nanowires

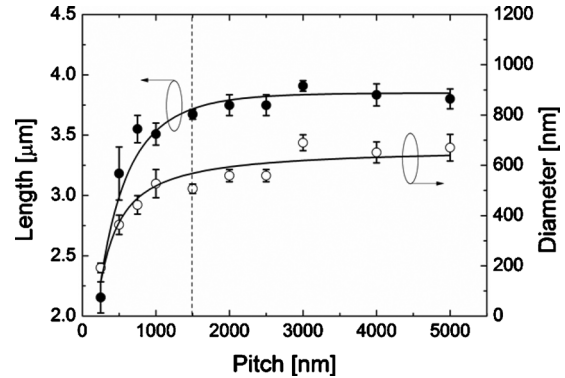


FIG. 7. Dependence of nanowire length and diameter as a function of pitch for a fixed growth time (360 min). The transition to saturation in both length and diameter (as deduced from best fits to the data) indicates the cross-over from a competitive growth regime to a diffusion-limited growth regime (illustrated by dotted line).

compete for adatoms to redistribute equally over the given nanowire density, which leads to a decrease in both vertical and radial growth rate. This rate-limiting *materials competition regime*, as previously examined also for GaP-based nanowires,<sup>43</sup> describes clearly the materials distribution under mass conservation over a fixed number of growing nanowires. According to this, increasing pitch corresponds to increased capture area for surface diffusing adatoms per individual nanowire which leads to increased growth rates, in agreement with our results.

On the other hand, when the surface diffusion length  $\lambda_{\text{SiO}_2}$  becomes less than one half of the pitch, the nanowires can be treated as independent isolated islands and growth is limited by the collection of the surface diffusing In adatoms. In this *diffusion-limited regime*, the growth rate therefore becomes independent of the pitch, resulting in completely identical rates, as confirmed here for pitches ranging from 1500–5000 nm. In this case, In adatoms which are not able to migrate further than the typical surface diffusion length cannot contribute to nanowire growth and either desorbed or form clusters on the  $\text{SiO}_2$  surface. Indeed, in selected SEM images we observed traces of clusters on the  $\text{SiO}_2$  surface for pitches larger than  $\sim 1500 \text{ nm}$ .

From the cross-over between the materials competition regime and the diffusion-limited growth regime we can determine the surface diffusion length  $\lambda_{\text{SiO}_2}$  under the given growth conditions. Since this cross-over occurred at a pitch of  $\sim 1.5 \mu\text{m}$ ,  $\lambda_{\text{SiO}_2}$  amounts, therefore, to  $\sim 750 \text{ nm}$  at the given growth temperature of  $480 \text{ }^\circ\text{C}$ . This is further corroborated in Fig. 7, showing the nanowire length and diameter dependence over a wide range of pitches resulting from a fixed growth time of 360 min. Clearly, both the nanowire length and diameter saturated at a pitch of around  $\sim 1.5 \mu\text{m}$ , in consistence with the previous growth rate analysis.

Moreover, despite the fact that the nanowires grown at the smallest pitches turned out to be the shortest in length, they simultaneously exhibited the largest aspect ratios (length/diameter), which even increased with growth time. This indicates that within the competitive growth regime direct impingement contributes significantly to vertical nanowire growth. This slows down the radial growth rate with

increasing time, leading further to shadowing effects where less and less impinging adatoms can arrive and diffuse from the substrate surface. In contrast, in the diffusion-limited growth regime the aspect ratios were found constant and independent of the selected pitch, meaning that here direct impingement plays no role.

#### IV. CONCLUSIONS

In summary, we established catalyst-free site-selective growth of vertically well-oriented, high yield InAs nanowire arrays on Si(111) by solid-source MBE. Important advantages of this growth approach were found in the independence of the vertical nanowire growth yield from prewetting conditions and the selected pitch (interwire distance), resulting in consistently high yields of  $\sim 90\%$ . We confirmed the excellent control of the vertical growth directionality by very low crystal tilt in x-ray rocking curve measurements. Systematic investigations of the size scaling behavior as a function of the interwire distance highlighted the existence of two growth regimes within the noncatalytic growth processes: (i) a competitive growth regime for low interwire distances governed by redistribution of In adatoms over multiple nanowires as well as direct impingement, and (ii) a diffusion-limited growth regime, where growth is limited by the surface diffusion length of In adatoms on the SiO<sub>2</sub> surface ( $\sim 750$  nm at the given growth conditions). Here, the radial and axial nanowire growth rates were found completely independent of the interwire distance, resulting in identical lengths and diameters. Most strikingly, over the large range of nanowire densities investigated, the underlying geometry (i.e., nanowire shape) remained unaltered. These findings provide an important step toward obtaining controlled nanowire growth necessary for designing highly reproducible III-V based vertical nanowire devices on Si platform.

#### ACKNOWLEDGMENTS

The authors thank E. Forster, F. Herzog, and S. Lindner for innumerable SEM measurements, A. W. Holleitner and P. Weiser for SEM support, and B. Laumer and M. Stutzmann for providing the XRD facilities. S. H. and D. R. also thank R. Meyer for support with ellipsometry. For helpful discussions we gratefully acknowledge M. Heiß (EPF Lausanne), N. Hauke (WSI), and L. Geelhaar (PDI Berlin). This work was supported by the Marie Curie FP7 Reintegration Grant (Christina Totté, project officer), the FP7 project SOLID, the DFG excellence program Nanosystems Initiative Munich, the collaborative research center SFB 631, and the TUM Institute of Advanced Study.

<sup>1</sup>M. S. Gudiksen, L. J. Lauhon, J. Wang, D. C. Smith, and C. M. Lieber, *Nature (London)* **415**, 617 (2002).

<sup>2</sup>L. J. Lauhon, M. S. Gudiksen, D. Wang, and C. M. Lieber, *Nature (London)* **420**, 57 (2002).

<sup>3</sup>Y. Huang and C. M. Lieber, *Pure Appl. Chem.* **76**, 2051 (2004).

<sup>4</sup>Y. Huang, X. Duan, Y. Cui, L. J. Lauhon, K.-H. Kim, and C. M. Lieber, *Science* **294**, 1313 (2001).

<sup>5</sup>B. M. Kayes, H. A. Atwater, and N. S. Lewis, *J. Appl. Phys.* **97**, 114302 (2005).

<sup>6</sup>C. Colombo, M. Heiß, M. Grätzel, and A. Fontcuberta i Morral, *Appl. Phys. Lett.* **94**, 173108 (2009).

<sup>7</sup>Z. Zhang, J. Y. Ying, and M. S. Dresselhaus, *J. Mater. Res.* **13**, 1745 (1998).

<sup>8</sup>A. I. Boukai, Y. Bunimovich, J. Tahir-Kheli, J. K. Yu, W. A. Goddard, and J. R. Heath, *Nature (London)* **451**, 168 (2008).

<sup>9</sup>G. F. Zheng, F. Patolsky, Y. Cui, W. U. Wang, and C. M. Lieber, *Nat. Biotechnol.* **23**, 1294 (2005).

<sup>10</sup>C. R. Bolognesi, E. J. Caine, and H. Kroemer, *IEEE Electron Device Lett.* **15**, 16 (1994).

<sup>11</sup>J. A. Lott, N. N. Ledentsov, V. M. Ustinov, N. A. Maleev, A. E. Zhukov, A. R. Kovsh, M. V. Maximov, B. V. Volovik, Zh. I. Alferov, and D. Bimberg, *Electron. Lett.* **36**, 1384 (2000).

<sup>12</sup>W. Wei, X. Bao, C. Soci, Y. Ding, Z. Wang, and D. Wang, *Nano Lett.* **9**, 2926 (2009).

<sup>13</sup>A. T. Mårtensson, C. P. Svesson, B. A. Wacaser, M. W. Larsson, W. Seifert, K. Deppert, A. Gustafsson, L. R. Wallenberg, and L. Samuelson, *Nano Lett.* **4**, 1987 (2004).

<sup>14</sup>S. D. Brotherton and J. E. Lowther, *Phys. Rev. Lett.* **44**, 606 (1980).

<sup>15</sup>Y. Wang, V. Schmidt, S. Senz, and U. Goesele, *Nat. Nanotechnol.* **1**, 186 (2006).

<sup>16</sup>A. L. Roest, M. A. Verheijen, O. Wunnicke, S. Serafin, H. Wondergem, and E. P. A. M. Bakkers, *Nanotechnology* **17**, S271 (2006).

<sup>17</sup>E. P. A. M. Bakkers, J. A. V. Dam, S. D. Franceschi, L. P. Kouwenhoven, M. Kaiser, M. Verheijen, H. Wondergem, and P. V. D. Sluis, *Nature Mater.* **3**, 769 (2004).

<sup>18</sup>S. A. Dayeh, E. T. Yu, and D. Wang, *Nano Lett.* **9**, 1967 (2009).

<sup>19</sup>K. Tomioka, P. Mohan, J. Noborisaka, S. Hara, J. Motohisa, and T. Fukui, *J. Cryst. Growth* **298**, 644 (2007).

<sup>20</sup>K. Tomioka, J. Motohisa, S. Hara, and T. Fukui, *Nano Lett.* **8**, 3475 (2008).

<sup>21</sup>Y. Ding, J. Motohisa, B. Hua, S. Hara, and T. Fukui, *Nano Lett.* **7**, 3598 (2007).

<sup>22</sup>K. Ikejiri, T. Sato, H. Yoshida, K. Hiruma, J. Motohisa, S. Hara, and T. Fukui, *Nanotechnology* **19**, 265604 (2008).

<sup>23</sup>Z. H. Wu, M. Sun, X. Y. Mei, and H. E. Ruda, *Appl. Phys. Lett.* **85**, 657 (2004).

<sup>24</sup>A. Lugstein, A. M. Andrews, M. Steinmair, Y. J. Hyun, E. Bertagnoli, M. Weil, P. Pongratz, M. Schrambock, T. Roch, and G. Strasser, *Nanotechnology* **18**, 355306 (2007).

<sup>25</sup>S. G. Ihn, J. I. Song, Y. H. Kim, J. Y. Lee, and I. H. Ahn, *IEEE Trans. Nanotechnol.* **6**, 384 (2007).

<sup>26</sup>A. Fontcuberta i Morral, D. Spirkoska, J. Arbiol, M. Heigoldt, J. R. Morante, and G. Abstreiter, *Small* **4**, 899 (2008).

<sup>27</sup>S. G. Ihn and J. I. Song, *Nanotechnology* **18**, 355603 (2007).

<sup>28</sup>G. Koblmüller, S. Hertenberger, K. Vizbaras, M. Bichler, J.-P. Zhang, and G. Abstreiter, *Nanotechnology* **21**, 365602 (2010).

<sup>29</sup>A. Okamoto, *Semicond. Sci. Technol.* **8**, 1011 (1993).

<sup>30</sup>X. F. Liu, H. Asahi, Y. Okuno, D. Marx, K. Inoue, and S. Gonda, *J. Cryst. Growth* **136**, 250 (1994).

<sup>31</sup>F. Allegretti, M. Inoue, and T. Nishinaga, *J. Cryst. Growth* **146**, 354 (1995).

<sup>32</sup>S. C. Lee, K. J. Malloy, and S. R. J. Brueck, *J. Appl. Phys.* **90**, 4163 (2001).

<sup>33</sup>M. Heiß, E. Riedberger, D. Spirkoska, M. Bichler, G. Abstreiter, and A. Fontcuberta i Morral, *J. Cryst. Growth* **310**, 1049 (2008).

<sup>34</sup>C. Colombo, D. Spirkoska, M. Frimmer, G. Abstreiter, and A. Fontcuberta i Morral, *Phys. Rev. B* **77**, 155326 (2008).

<sup>35</sup>H. D. Park, S. M. Prokes, M. E. Twigg, R. C. Cammarata, and A.-C. Gaillot, *Appl. Phys. Lett.* **89**, 223125 (2006).

<sup>36</sup>J. R. Arthur, *J. Appl. Phys.* **37**, 3057 (1966).

<sup>37</sup>W. I. Park, D. H. Kim, S.-W. Jung, and G.-C. Yi, *Appl. Phys. Lett.* **80**, 4232 (2002).

<sup>38</sup>X. Han, G. Wang, Q. Wang, L. Cao, R. Liu, B. Zou, and J. G. Hou, *Appl. Phys. Lett.* **86**, 223106 (2005).

<sup>39</sup>A. Portavoce, R. Hull, M. C. Reuter, and F. M. Ross, *Phys. Rev. B* **76**, 235301 (2007).

<sup>40</sup>L. E. Jensen, M. T. Björk, S. Jeppesen, A. I. Persson, B. J. Ohlsson, and L. Samuelson, *Nano Lett.* **4**, 1961 (2004).

<sup>41</sup>R. L. Headrick, S. Kycia, and Y. K. Park, *Phys. Rev. B* **54**, 14686 (1996).

<sup>42</sup>G. Koblmüller, P. Pongratz, R. Averbeck, and H. Riechert, *Appl. Phys. Lett.* **80**, 2281 (2002).

<sup>43</sup>M. T. Borgström, G. Immink, B. Ketelaars, R. Algra, and E. P. A. M. Bakkers, *Nat. Nanotechnol.* **2**, 541 (2007).